Applied Materials Today 25 (2021) 101233

Contents lists available at ScienceDirect

Applied Materials Today

journal homepage: www.elsevier.com/locate/apmt

Multi-scale cold embossing of CoCrFeNiMn high entropy alloy with ultra-high temperature durability

Wenxin Wen, Zhiyuan Huang, Zhen Li, Jianan Fu, Wenqing Ruan, Shuai Ren, Zhenxuan Zhang, Xiong Liang, Jiang Ma*

Shenzhen Key Laboratory of High Performance Nontraditional Manufacturing, College of Mechatronics and Control Engineering, Shenzhen University, Shenzhen, 518060, China

ARTICLE INFO

Article history:
Received 15 August 2021
Revised 26 September 2021
Accepted 15 October 2021

Keywords:
High entropy alloys
Cold embossing
Multi-scale deformation
Ultra-precision machining

ABSTRACT

Ultra-precision machining and forming of metallic materials is of great significance in the fields of catalysts, sensors, and biomedical devices. In present work, the multi-scale cold embossing of CoCrFeNiMn high entropy alloy (HEA) with structures ranging from macro-scale to nano-scale was investigated at room temperature. In less 7 s, the macro patterns, the shapes of Arabic numerals, 5 μm wide gratings, 30 μm diameter hemispherical arrays, and ~270 nm nanowires were formed rapidly. The highest replication of the HEA cold embossing was up to 98%. A series of slip bands were detected in the cold embossed HEA structures, which can accommodate more dislocations and facilitate the plastic deformation process. Moreover, dislocation pile-up and large angular rotation within grains are observed in the deformation areas, which is favorable to contain dislocation cells, leading to grain refinement and an increase in hardness. In addition, the multi-scale HEA can be used as a high-temperature resistant mold for forming thermoplastic materials such as plastics and metallic glasses at temperatures up to 900 °C. Our researches provide candidate materials and novel methods for the facile preparation and various applications of hyperfine structures.

1. Introduction

Precision and ultra-precision machining is the basis and key of advanced manufacturing technology. Precision machining technology has greatly improved the level of the machinery manufacturing industry, strongly supports the development of other industries with remarkable achievements in the automobile manufacturing industry and microelectronics industry. For example, the design and manufacture of integrated circuits which belong to the high-tech field cannot be achieved without the precision progressive molds of lead frames and the precision plastic films of integrated circuits [1]. The manufacture of calculator shells, plugins, and many components must also use precision plastic molds and stamping molds [2]. The development of digital electronic products, including communication products, cannot be separated from precision molds. Mold industry is an important field of high-tech industrialization. The progress of mold manufacturing technology and industrial technology is inseparable from the high-tech industry. However, the existing preparation technology of micro and nano-scale structures has disadvantages of high cost and complex preparation technology. Therefore, it is of great significance to develop new materials and methods to make molds and functional devices.

High Entropy Alloys (HEAs), a class of multi-component alloys with equimolar ratio, were independently proposed in 2004 [3, 4]. The four core effects, including the high entropy effect, the lattice distortion effect, the slow diffusion effect and the cocktail effect, exclusive belong to HEAs [5, 6]. The solid solution strengthening mechanism of HEAs is very significant. When the crystal structure of the multi-component HEAs is a solid solution, because of the variety of elements, the differences between the atomic radius of each principal element, the randomness of the occupied lattice the HEAs has an obvious solid solution strengthening effect. HEAs have obvious solid solution strengthening effects due to the diversity of elements, the difference of atomic radii of each main element, and the randomness of the occupied lattice. Because of the unique strengthening mechanism and structures of HEAs, it has high strength and hardness [4], excellent corrosion resistance [7, 8], good thermal stability [9, 10], high fatigue resistance [6, 11], excellent wear resistance [12, 13], good chemical catalytic performance [14], good radiation resistance [15, 16] and so on. Some kinds of HEAs exhibit good plasticity [17], which makes them possible to fabricate the hyperfine microstructures at even room tem-

* Corresponding author.
E-mail address: majiang@szu.edu.cn (J. Ma).

https://doi.org/10.1016/j.apmt.2021.101233
2352-9407/

perature. Not only that, different from other precious metals, the material mentioned in this paper is a kind of potential material and easy to industrial. Compared with 3D printing and other methods of manufacturing mold, this kind of material with this method is easier to be made into many different complex structures in less time. In addition, the multi-scale structures have great effects on the catalytic degradation process. By controlling the morphology of materials, highly active materials can be designed and developed to achieve photocatalytic degradation, microstructure control and other functions [18].

The CoCrFeNiMn HEA is a kind of very scientific and interesting material. Five of its elements crystallize in different forms, but it shows a single-phase plane-centered cubic structure [19]. This is the reason for the high ductility and excellent low-temperature properties of this material [20]. Moreover, due to the size effect in the processing of many materials, the properties of materials change greatly. Therefore, multi-scale molding plays an important role in the development of science. Nowadays, there are few studies on the multi-scale molding of HEA, especially at the micro and nano-scale at room temperature. In this paper, the multi-scale cold embossing of HEA, including macro-scale, micro-scale and nano-scale molding of the material, is investigated. And the mechanism that induces room temperature plastic forming ability was explored. Finally, the material properties after molding were studied and the potential applications were proposed. This is an important ground-breaking and significant in key fields such as multi-scale manufacturing and micro tools.

2. Materials and methods

2.1. Materials

The equiatomic CoCrFeNiMn HEA was produced from elements with a purity of 99% (at.%) by vacuum-induction melting. The ingots were cut into 10 mm in length, 10 mm in width, and 1 mm in height by wire electrical discharge machining-low speed (WEDM-LS). The 5 mm diameter samples were also prepared in the same way, with heights of 1 mm and 2 mm, respectively. Then, the sample surfaces were polished by a polishing machine with 800, 1200, 1500 meshes sandpaper and velvet polishing cloth.

2.2. Cold embossing experiment of HEA

The multi-scale structures were prepared by a self-made pressing machine at room temperature. The macrostructures were fabricated using a stainless-steel mold at a pressure load of 30 kN and a speed of 0.07 mm/s, 0.1 mm/s and 1 mm/s, respectively. The glass grating with a slot width of 30 μm and a nickel template with an array of various shapes were used as a mold for fabricating the microstructures, and the porous Anodized Aluminum Oxide (AAO) templates with diameters of 200 nm and 300 nm were used as molds for nanostructures. All of the above actions are pressed to the set value and held for a period time of 5 s.

2.3. Characterization

The HEA microstructure nature was ascertained by x-ray diffraction (XRD, Rigaku-miniflex 600, Japan) test in a 2θ range of 20° to 100° at a scan rate of 5° per minute and a scan-interval of 0.02° with the Cu Kα radiation with a wavelength of 0.154 nm.

The molding structures were observed by a scanning electron microscope (SEM; Hitachi-SU70, Japan) with low magnification. By comparing the molded samples and molds under SEM, the molding quality can be observed. The two comparison samples before and after the shape were cut into small pieces.

Transmission electron microscopy (TEM, Fei Titan Themis) with energy dispersive spectroscopy (EDS) was used for microstructure and phase analysis. The HEA samples were prepared by SEM/FIB double beam system (FEI SCIOS). The crystalline atom arrangement, interface microstructure and surface element distribution were obtained by the High-Angle Annular Dark Field (HAADF) and selected area electron diffraction images taken by HEA with double spherical aberration correctors (Cs-STEM).

The microstructure evolutions in the deformation area of the samples were characterized by electron backscattered diffraction (EBSD) equipped with an HKL-EBSD system, using the TESCAN MAIA3 scanning electron microscope. The sample was prepared by 6.5 kV ion beam polishing for 1 h. The step size of electron beam diffraction character shaping at 20 kV was 0.5 $\sim$ 2 m, and the obtained data were analyzed by using Oxford HKL Channel 5 software (Oxford Instruments). The local directional errors of the deformation zone were determined based on the kernel mean directional error (KAM).

The compression was conducted on the mechanical testing machine (Zwick Roell Z050 TEW). The characteristics of plasticity were measured by a universal tensile testing machine with 30 kN and 0.07 mm /s.

An automatic Vickers hardness tester is held for 10 s at the load of 500 gf (4.90 N) to measure the surface hardness of the cross-section. The samples before and after cold embossing were tested three times with fifteen indents each. For the original sample, the average interval of each indent is 200 um. At the same time, the indents selected for the cold-embossed sample were taken from three different characters in the text area of the macro-scale samples, with 5 points for each character and an average interval of 200 um for each indent. Then, the data from each section were averaged.

2.4. Heat treatment

The HEA sample after cold embossing at room temperature was placed in a self-made hot-embossing device and heated to 500 °C at a rate of 10 °C per minute in a high vacuum environment. Then, the quenching process was realized through the quick cooling device in the self-made hot embossing device. After cooling for 10 min in a low vacuum environment, the sample was taken and placed at room temperature for further cooling. Also, The HEA sample was placed in the device and heated to 800 °C at a rate of 10 °C per minute. It is then cooled to 650 °C with the furnace. Subsequently, the quenching process was realized too. After cooling for 20 min in a low vacuum environment, the sample was taken and placed at room temperature for further cooling.

2.5. Hot embossing experiment of thermoplastic materials

The multiscale structure was prepared by using HEA samples as molds under a self-made hot embossing device. First, the temperature was heated to the T_g of PMMA, and then apply pressure of 1 kN at the feed rate of 0.1 mm/s. When the deformation of 0.1 mm occurs, the pressure is stopped and the sample is taken out after cooling. In the same way, the $La_{55}Al_{25}Ni_5Cu_{10}Co_5$ MG samples can replicate structures of HEA molds.

3. Results and discussion

3.1. Cold embossing and replicate of HEA structures

It is found that the CoCrFeNiMn HEA has a good plastic forming ability and can be molded into various patterns at room temperature. Fig. 1a shows a schematic diagram of cold embossing at room temperature. The complete cold embossing process is very simple,

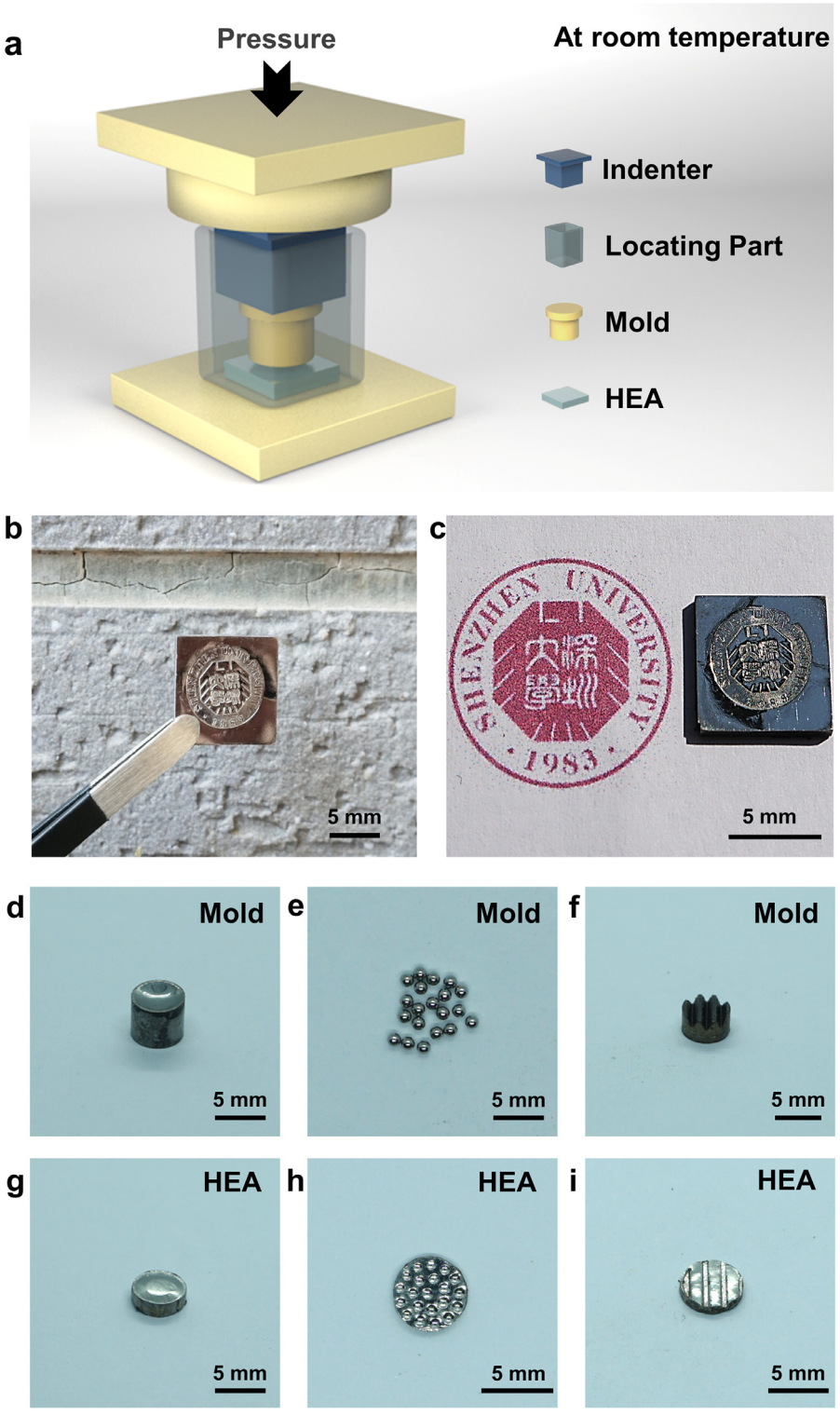

Fig. 1. Schematic diagram and the macro-scale structure of cold embossing. (a) Schematic diagram of cold embossing, (b) the macroscopic structure of cold embossing, (c) comparison diagram of macroscopic embossing structure and mold graphic, (d-f) Mold of macro-scale structure, and materials are tungsten steel YG8 and SKD61, (g-i) HEA samples are copied with the mold of (d-f) using the cold embossing.

that is, the mold, the sample and the indenter are placed in the limiting mold one by one, and the pressure is applied vertically downward to the top of the indenter. Finally, the sample is separated from the mold easily, and the desired product with the mold structure is obtained. Therefore, macro-scale patterns are produced by this simple cold embossing method. It should be noted that the cold embossing process was finished in less than 7 s at room temperature. The patterns of the specific logo in Fig. 1b and c are the results of cold embossing with stainless steel mold, illustrating the integrity of the replicated pattern. If the difference in the depth of the sample impression is to be obtained, it can be achieved by adjusting the pressure and feed rate. When compared with the photo

which represents enlarged the pattern on the mold in Fig. 1c, one can find that there is an accurate replication between the mold and the replica. In addition, other macro-scale structures can also be easily prepared using the molds (Fig. 1d, e and f), as shown in Fig. 1g, h and i. In a sense, due to the formability of the material and process, it provides a superior candidate material for the molding process. This not only provides a way to manufacture crafts, but also can be used as a mold for some special functions and complex structures.

Furthermore, the micro-scale and nano-scale forming abilities were also investigated at room temperature. Fig. 2a shows the schematic diagram of the micro-scale cold embossing process at room temperature. The HEA is stacked on top of the mold, vertical downward pressure is applied on top, then the HEA is demolded, resulting in a sample that precisely replicates the micro-scale structures on the mold. A Nickel template with micro-scale digital shapes (Fig. 2b) and hemispherical arrays (Fig. 2c) were used as molds to form HEA. In addition, a glass grating template with grooves width of 5 μm was used to prepare micro-scale structures (Fig. 2d). Fig. 2e, f, and g are the micro-scale structures on HEA after cold embossing, which can be clearly compared with the structures on the mold in Fig. 2b, c, and d, respectively. Then, by comparing Fig. 2b and e, it can be seen that the sample accurately duplicates the shape of the Arabic numerals on the original mold, and the partially enlarged image shows the numerical details on the mold precisely. As can be seen from Fig. 2c and f, the hemispherical arrays on the mold are well duplicated by the sample. By measuring the upper circle diameter of the hemispherical arrays of mold and the bottom circle diameter of the HEA, they were 30 μm and 31 μm, respectively. That is to say, the replication accuracy reaches as high as 97%. In addition, the grooves in the grating in Fig. 2d and g have widths of 5 μm and 5.1 μm, respectively, with a replication accuracy of 98%.

Next, the nano-scale formation of HEA at room temperature was further investigated. Fig. 2h schematically shows the schematic diagram of nano-scale cold embossing at room temperature. The AAO templates with nanopores were used as molds in this stage. To exclude the influence of the template and reveal the true morphology of the HEA, the samples were removed by immersion in 10% NaOH solution heated at 80 °C for 30 min. The nano-scale structures of HEA were observed by SEM and the results are shown in Fig. 2i, j, and k, respectively. The SEM images show that large-area of nanowires are prepared, and the aspect ratio of some nanowires reaches 5:1, which proves that HEA also showed good nano-scale forming ability at even room temperature. From this, we can conclude that by cold embossing HEAs at macroscale, microscale and nanoscale, it can be found that they can accurately replicate the shape, size and roughness of the mold at different scales. The excellent room-temperature plastic forming capability of this material offers new options for functional forming, which is important for the fabrication of multi-scale molds.

3.2. Characterization and cold forming mechanism

In order to unveil the deformation mechanism, we deeply observed the structures of the deformation area. First, the surface of the array shape formed at the micro-scale due to cold plastic deformation under SEM can be observed, as shown in Fig. 3a. Then, a region in Fig. 3a was enlarged, in which a large number of wrinkles are found on the HEA sample surface, as shown in Fig. 3b. Subsequently, the phenomenon (Fig. 3c) observed under TEM further confirms the existence and distribution of dense dislocations. In addition, Fig. 3d shows a high-resolution TEM (HRTEM) image of a lamellar area near the dislocations. And one-dimensional inverse-FFT images in Fig. 3e and f reveal the different sets of planes. A large number of dislocations are observed and marked by the symbol $\perp$. It's worth noting that there are more dislocations in Fig. 3e than these in Fig. 3f, indicating that the preferred orientation of the grains in the crystal was formed during the cold plastic deformation. This can also be seen in XRD patterns before and after deformation (see Fig. S1 in the supplementary materials). These dislocations may be caused by the uneven distribution of impurity atoms in the solidification process and the local stress concentration when the crystal is subjected to a force. Then, EDS was used to map elemental distribution near the dislocations. From the EDS image (Fig. 3g), it proves that there are no appreciable compositional variations in the dislocation area. And the element distribution line chart in Fig. S2 (supplementary materials) shows that the chemical composition of the five constituent elements remains nearly equiatomic.

Obviously, the HEA has good plasticity at room temperature (see Fig. S3 in the supplementary materials), so it can be molded into a variety of patterns with different length scales. In crystalline metals, different plastic deformation mechanisms, such as dislocation-mediated plasticity [21, 22], twinning [23], grain boundary slip, or rotation [24, 25], will occur due to different grain sizes. In our experimental materials, the size of molds used at different scales far exceeds the grain size, so the slip and rotation of grain boundary are not the main reasons for the dominant plastic deformation [26, 27]. For coarse-grained FCC metals, the deformation mechanism at low temperatures is usually dominated by dislocation [22]. Through a series of analyses, the forming mechanism at room temperature plastic deformation of high entropy alloy is temporarily locked as dislocation-induced plastic deformation.

In order to further confirm the mechanism of the dislocation-induced plastic deformation, the evolution of the microstructure was further observed. From a crystallographic perspective, two EBSD maps in Fig. 3h and i show the comparison before and after the cold plastic deformation. Different colors on the Figures show different preferred orientations, indicating that the preferred orientations of each grain are produced under cold plastic deformation. Not only that, it can be clearly seen that in Fig. 3h, three positions are arbitrarily taken in a grain along the direction of arrow A, and the rotation angles of coordinate axes are basically the same. However, it can be seen from Fig. 3i that when three positions are taken along the direction of arrow B, it can be found that the third coordinate axis of the second position rotates by about 80° compared with the other two positions. In these two Figures, it can be found that the grain orientation has been changed in a grain due to cold plastic deformation. That means the entire process of cold embossing at room temperature generates the dislocations causing a small amount of deflection of the lattice and the formation of small-angle grain boundaries. The dislocation source on the slip surface opens up and the dislocation moves along the slip surface as plastic deformation occurs in the grains with favorable dislocation orientation. However, dislocations cannot cross grain boundaries to develop into adjacent grains, so dislocations are blocked at grain boundaries to form dislocation pile-ups. After the superposition of the dislocation pile-ups and the applied load, the tangential stress in the adjacent grains on some slip surfaces reaches a critical value, the slip system opens and the plastic deformation continues. According to the sharp contrast between before and after the cold plastic deformation shown in Fig. S4 (supplementary materials), it can be seen an increase of Schmid factor, which means that the slip system is easier to open and the plastic deformation is more likely to occur. At the same time, a large number of small-angle grain boundaries were found in Fig. S5 (supplementary materials), which confirmed the existence of a large number of slip bands and dislocation pile-ups. In addition, no serrated-flow phenomenon was found in CoCrFeNiMn HEA during the deformation at room temperature, which may be due to the low diffusion ve-

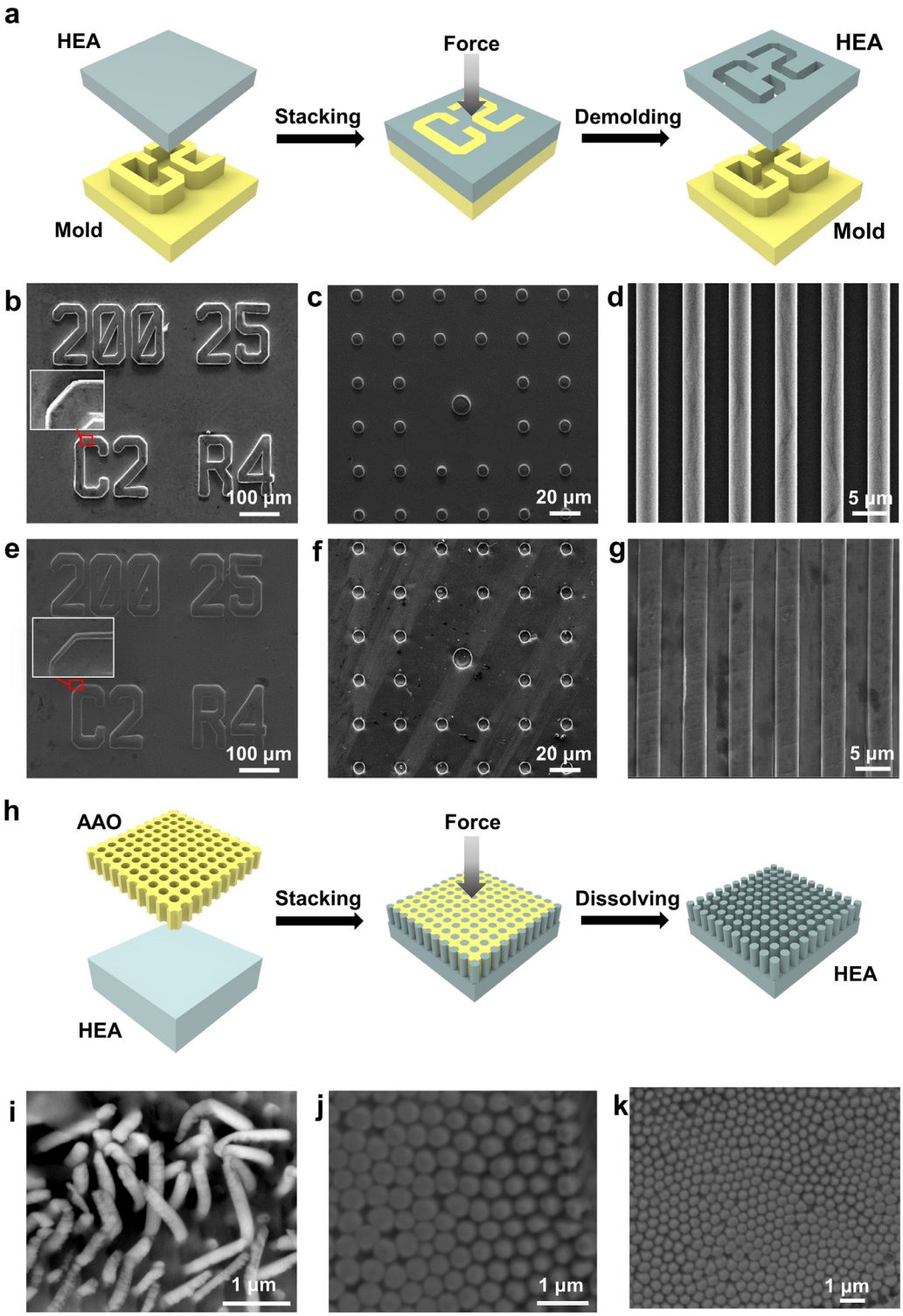

Fig. 2. Micro-scale and nanoscale structures of cold embossing. (a) Micro-scale schematic diagram of cold embossing, (b-d) The SEM images of micro-scale structures on mold, (e-g) The SEM images of micro-scale structures on HEA, (h) Nano-scale schematic diagram of cold embossing, (i-k) The SEM images of nano-scale structures on HEA.

locity of solute atoms that cannot lock the dislocation movement [28].

It can be inferred that the HEA has a very low stacking fault energy, which is conducive to the accumulation of defects in the deformation process, because the low stacking fault can lead to dislocation dissociation, and the spacing between dislocations is large. This allows more defects to be accommodated in the large spacing of dislocations, allowing deformation to continue. When a large number of such defects accumulate to a certain extent, This in turn severely inhibits cross slip of helical dislocations [29]. At the same time, elongated grain boundaries accumulate, and as the deformation continues, the grains are elongated, resulting in further width reduction and eventually grain boundary collapse [28]. This will result in the generation of new grain boundaries (see Fig. 6 in supplementary materials), which will then lead to grain refinement and accommodates the dislocation pile-ups.

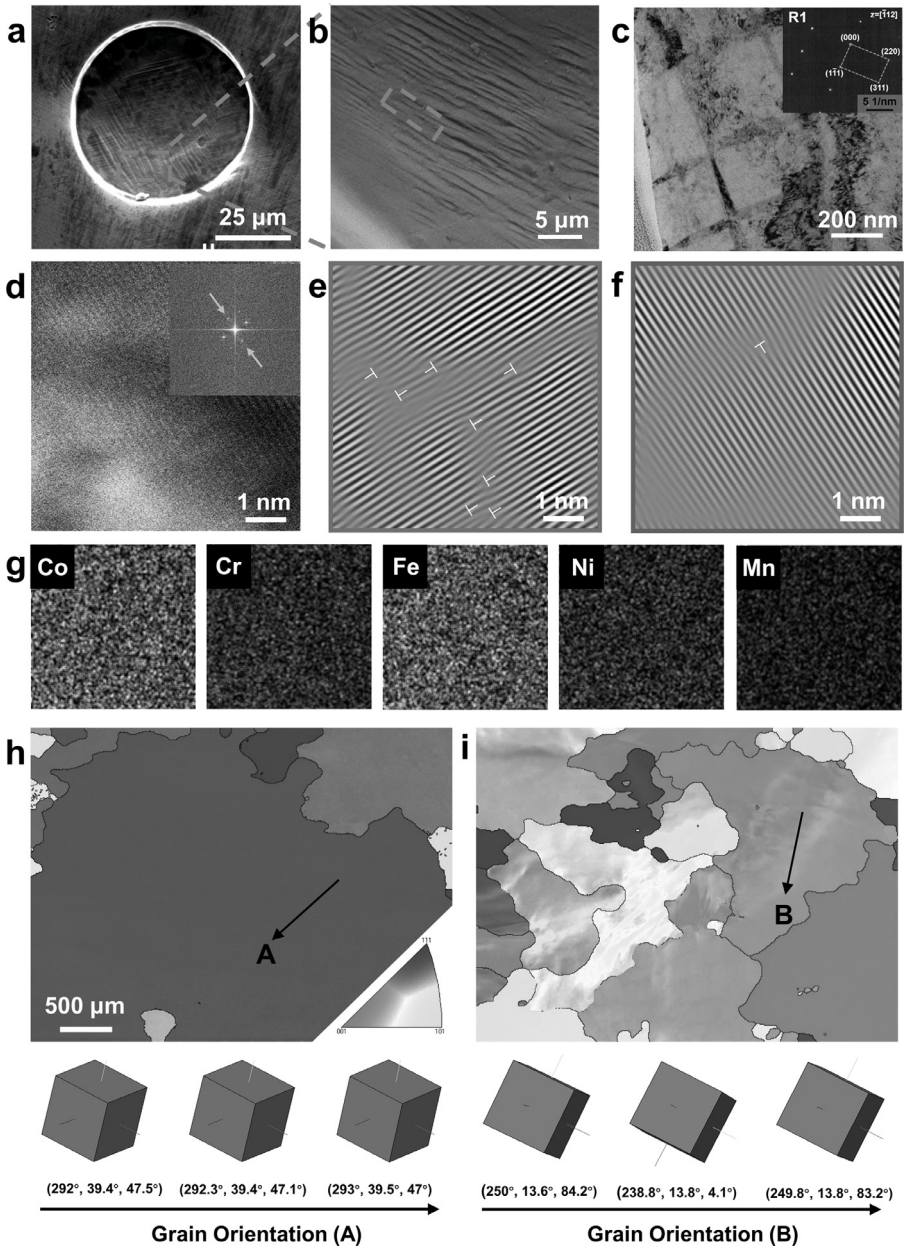

Fig. 3. Evolution and characterization of microstructures. (a-b) SEM images of Sliding bands in microstructure, (c) TEM image of the dislocation distribution d, HRTEM image of a typical area, (e-f) One-dimensional Fourier-filtered image of the squared area in (d), (g) Element distribution of the composite at the interface, (h-i) the EBSD images of grain orientation spread and internal crystal rotation before and after deformation.

3.3. Highlight advantages and potential applications

As a metal alloy, CoCrFeNiMn HEA has better room temperature plastic forming ability compared with other materials. In this work, the process of cold embossing often takes only a few seconds. That means the formation of HEA can be conducted at room temperature with high production efficiency. In addition, alloys can be used in certain applications because they have some properties that are better than pure metallic elements. After the plastic deformation of the material of cold embossing, the work hardening phenomenon can be easily detected. According to the results of the microhardness tester, the Vickers hardness of the material after the deformation is increased by 25% (see Fig. S7 in supplementary materials). For as-cast HEA, pressure machining can improve casting defects such as shrinkage, porosity and internal microstructure. In the plastically deformed alloy, a large number of dislocations will occur inside the grain, which further strengthens the solution strengthening effect [30, 31]. Trough the cold embossing method, the CoCrFeNiMn HEA achieves surface modification, resulting in the improvement of mechanical properties.

Fig. 4 shows the comparison of CoCrFeNiMn HEA with different materials including pure metal, traditional alloys, metallic glasses (MGs), ceramics and polymers (see Table S1 in supplementary materials). Different from the traditional alloys, the formation of CoCrFeNiMn HEA is at room temperature, which can prevent some new secondary phases precipitates after hot deformation, indicating that the CoCrFeNiMn HEA has excellent room temperature properties. Moreover, in order to prepare the micro-scale even nano-scale structures, traditional alloys require high temperatures, because the phase transformation time is optimal for embossing [32]. Due to the limitation of the inherent characteristic of metal, for instance, the size of grains, the size of micro-scale deformation

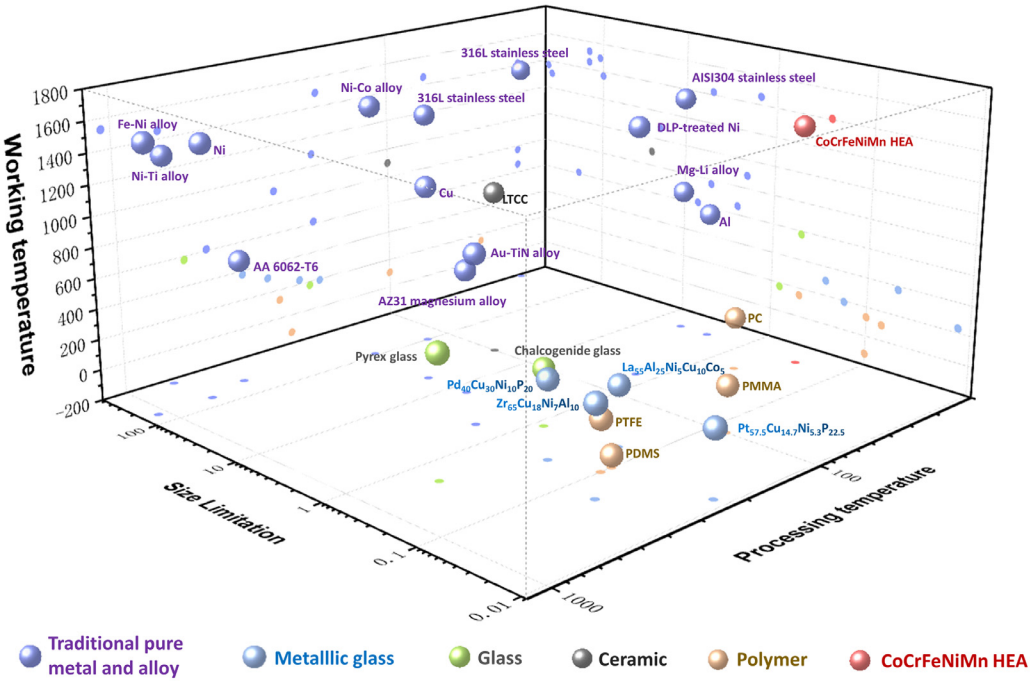

Fig. 4. Three-dimensional scatter image for CoCrFeNiMn HEA in relation to a wide range of material systems.

is limited [33, 34]. With hot embossing process, although some micro-scale structures can be achieved with glasses, the demolding process is more difficult because of the vicinity [35]. And the low mobility of ceramics leads the incomplete filling [36]. However, the unique characteristics of CoCrFeNiMn make the deformation at room temperature easier, and the limiting size is small (~270 nm). It is known that polymer is a kind of ideal material to prepare the micro-scale and nano-scale structures. But compared with the mold made by CoCrFeNiMn HEA, it does not have excellent mechanical properties, high using temperature and long service life. MG has excellent thermoplasticity enabling the molding of ultrafine structures at certain temperatures [37–39], and also possesses excellent mechanical and catalytic properties [40, 41]. But they are easy to get crystallized at temperatures above the crystallization point, resulting in the limitation of using temperature. Therefore, the CoCrFeNiMn HEA owns the high-temperature performance, simple manufacturing process and good mechanical properties.

So as to explore the application of this material, the samples prepared in the previous experiments were used as molds. The ideal samples that were used for hot embossing included MG and polymethyl methacrylate (PMMA) [42–45], because of their thermoplastic forming performance. As seen in Fig. 5a, it shows the schematic diagram of hot embossing. The samples prepared by cold embossing in the previous experiment were stacked with the thermoplastic material. The temperature is raised to the glass transition temperature (T_g) of the thermoplastic material and a small amount of pressure is applied. After cooling and demolding, the duplicated samples with structures of CoCrFeNiMn HEA can be prepared. Then, the comparison of the HEA mold, MG sample and PMMA sample can infer the feasibility of CoCrFeNiMn HEA as molds (Fig. 5b-g). It is proved that the HEA is an ideal material to make macro-scale, micro-scale and nano-scale structures, resulting in that it exists many potential applications, such as mold industry. Not only that, the high-temperature properties of HEA are also excellent. The comparisons of the untreated HEA sample and the sample after heat treatment in 500 °C and 900 °C are depicted in Fig 5h, i and j, respectively. It is obvious that the sample after heat treatment still keeps the complete structures, and the shapes and surface quality almost remain unchanged, indicating that the CoCrFeNiMn HEA has excellent thermal stability. This demonstrates the feasibility of HEA as a mold even a high-temperature mold. In addition, HEAs has good fatigue resistance because of its unique structure and size effects, which can be useful in applications that require cyclic loading, such as aerospace industry [46]. The high irradiation resistance and corrosion resistance of HEAs are benefit to the applications in the nuclear industry, such as potential candidates for nuclear fuel and high-pressure vessel cladding materials [6]. To sum up, the CoCrFeNiMn HEA is a potential structural and functional material with wide application prospect.

4. Conclusion

We proposed a facile cold embossing method for CoCrFeNiMn HEA to fabricate multi-scale structures at room temperature. The macroscopic patterns, 5 μm wide gratings, 30 μm diameter hemispherical arrays and nanowires of CoCrFeNiMn HEA have been formed by cold embossing within 7 s. The room temperature superplastic forming mechanism can be proved by the TEM and EBSD characterizations. At room temperature, a series of slip bands and grain internal rotation in the HEA deformation areas can accommodate high-density dislocations and facilitate grain refinement, which enhances the plasticity of deformation during the rapid embossing process. The analysis shows that the HEA has excellent plastic forming ability and forming quality at room temperature. Our work not only studies the multi-scale molding of HEA from macro-scale to nano-scale but also explores the application of the embossed HEA as high-temperature-durability molds for the structural forming of thermoplastic materials. Our researches open a new way for the precision forming and applications of high entropy alloys.

Supplementary materials

The XRD curve of the untreated sample and the embossing sample; The element distribution line chart of cold embossing

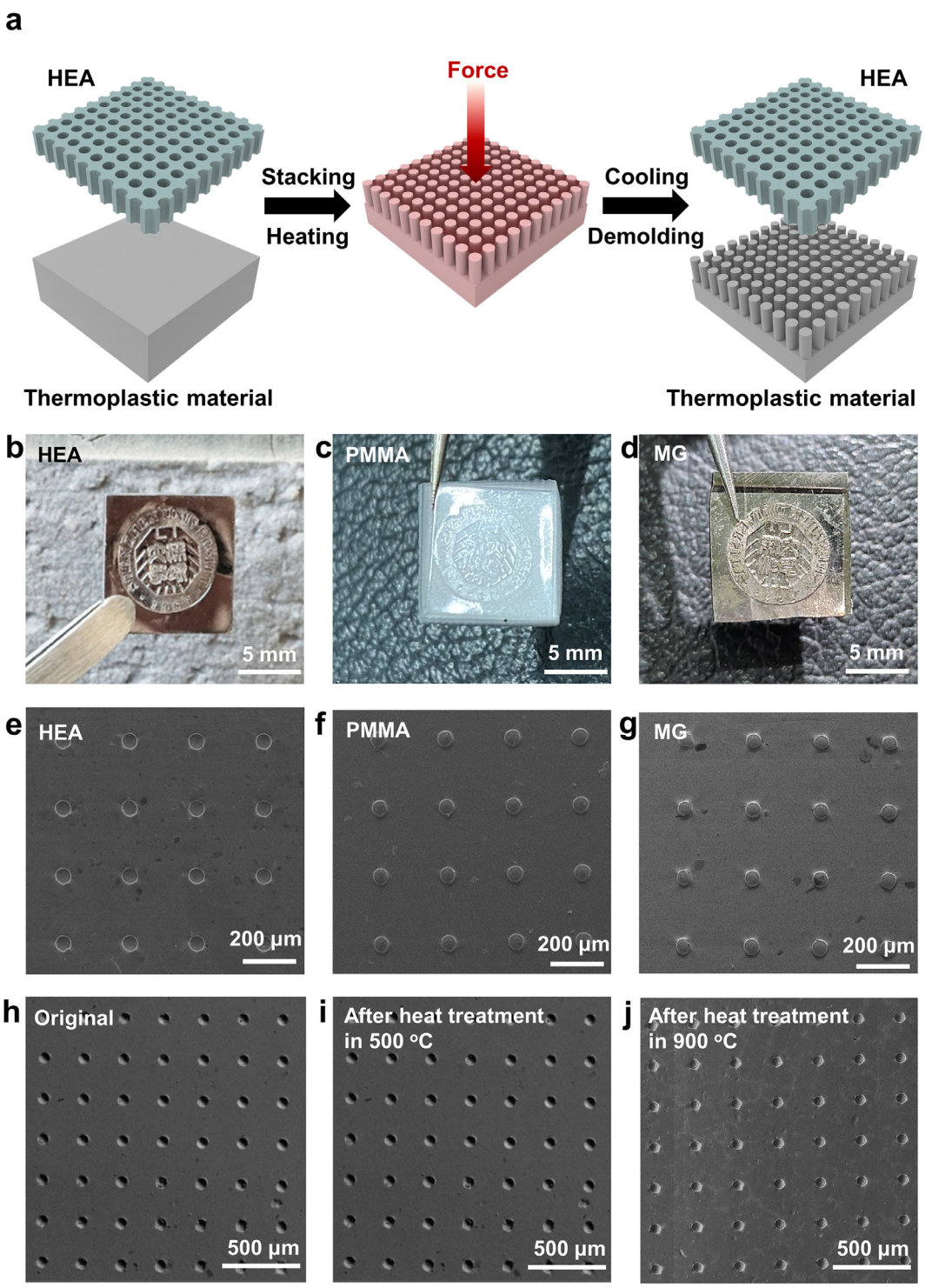

Fig. 5. Functional applications of CoCrFeNiMn HEA. (a) The schematic diagram of hot embossing, (b) the image of HEA mold with the positive logo pattern, (c-d) The PMMA and MG replica of (b) with the inverted logo pattern, (e) The SEM image of micro-scale structures of HEA mold with concave hemispherical array, (f-g) The SEM images of the PMMA and MG replica of (e) with a convex hemispherical array, (h-j) The SEM images of micro-scale structures of HEA before and after heat treatment.

sample; The stress-strain curve of CoCrFeNiMn HEA; Change of Schmid Factor during the plastic deformation; The difference of local misorientation before and after deformation; The EBSD images of Grain Orientation Spread before and after deformation; The difference of microhardness before and after deformation; and Comparison of using temperature, embossing temperature and limited size of CoCrFeNiMn HEA and a wide range of material systems.

Declaration of Competing Interest

The authors declare that they have no known competing financial interests or personal relationships that could have appeared to influence the work reported in this paper.

CRediT authorship contribution statement

Wenxin Wen: Data curation, Writing – original draft. **Zhiyuan Huang:** Investigation. **Wenqing Ruan:** Formal analysis. **Zhenxuan Zhang:** Supervision. **Xiong Liang:** Supervision. **Jiang Ma:** Writing – review & editing.

Acknowledgments

The work was supported by the National Key Research and Development Program of China (Grant No. 2018YFA0703604), the Key Basic and Applied Research Program of Guangdong Province, China (Grant Nr. 2019B030302010), the NSF of China (Grant Nr. 52122105, 51871157, 51971150). The authors also thank the assistance on microscope observation received from the Electron Microscope Center of the Shenzhen University.

Supplementary materials

Supplementary material associated with this article can be found, in the online version, at doi:10.1016/j.apmt.2021.101233.

References

[1] C. Robert, Devices for welding of integrated-circuit wafers, US (1975).
[2] K. Qin, L.I. Jie, B. Jiang, Forming process analysis of calculator shell and the injection mould design, Die Mould Ind. (2018).
[3] B. Cantor, I.T.H. Chang, P. Knight, A.J.B. Vincent, Microstructural development in equiatomic multicomponent alloys, Mater. Sci. Eng. 375-377 (2004) 213–218 http://dx.doi.org/, doi:10.1016/j.msea.2003.10.257.
[4] J.W. Yeh, S.K. Chen, S.J. Lin, J.Y. Gan, T.S. Chin, T.T. Shun, C.H. Tsau, S.Y. Chang, Nanostructured high-entropy alloys with multiple principal elements: novel alloy design concepts and outcomes, Adv. Eng. Mater. (2004) http://dx.doi.org/, doi:10.1002/adem.200300567.
[5] D.B.M. A, O.N.S.A. B, A critical review of high entropy alloys and related concepts, Acta Mater. 122 (2017) 448–511 http://dx.doi.org/, doi:10.1016/j.actamat.2016.08.081.
[6] Y. Zhang, T.T. Zuo, Z. Tang, M.C. Gao, K.A. Dahmen, P.K. Liaw, Z.P. Lu, Microstructures and properties of high-entropy alloys, Prog. Mater. Sci. 61 (2014) 1–93 http://dx.doi.org/, doi:10.1016/j.pmatsci.2013.10.001.
[7] C. Huang, Y. Zhang, J. Shen, V. Rui, Thermal stability and oxidation resistance of laser clad TiVCrAlSi high entropy alloy coatings on Ti–6Al–4V alloy, Surf. Coat. Technol. 206 (6) (2011) 1389–1395 http://dx.doi.org/, doi:10.1016/j.surfcoat.2011.08.063.
[8] C. Huang, Y. Zhang, V. Rui, J. Shen, Dry sliding wear behavior of laser clad TiVCrAlSi high entropy alloy coatings on Ti–6Al–4V substrate, Mater. Des. 41 (none) (2012) 338–343 http://dx.doi.org/, doi:10.1016/j.matdes.2012.04.049.
[9] O. N, and Senkov, G. B, and Wilks, D. B, and Miracle, C. P, Refractory high-entropy alloys, Intermetallics 18 (9) (2010) 1758–1765 http://dx.doi.org/, doi:10.1016/j.intermet.2010.05.014.
[10] O.N. Senkov, G.B. Wilks, J.M. Scott, D.B. Miracle, Mechanical properties of Nb25Mo25Ta25W25 and V20Nb20Mo20Ta20W20 refractory high entropy alloys, Intermetallics 19 (5) (2011) 698–706 http://dx.doi.org/, doi:10.1016/j.intermet.2011.01.004.
[11] Z. Wang, C. Wang, Y.-L. Zhao, Y.-C. Hsu, C.-L. Li, J.-J. Kai, C.-T. Liu, C.-H. Hsueh, High hardness and fatigue resistance of CoCrFeMnNi high entropy alloy films with ultrahigh-density nanotwins, Int. J. Plast. 131 (2020) 102726.
[12] J.M. Wu, S.J. Lin, J.W. Yeh, S.K. Chen, H.C. Chen, Adhesive wear behavior of AlxCoCrCuFeNi high-entropy alloys as a function of aluminum content, Wear 261 (5–6) (2006) 513–519 http://dx.doi.org/, doi:10.1016/j.wear.2005.12.008.
[13] C.-Y.H. a, T.-S.S. b, J.-W.Y. a, S.-K.C. c, Effect of iron content on wear behavior of AlCoCrFe x Mo 0.5 Ni high-entropy alloys, Wear 268 (5–6) (2010) 653–659 http://dx.doi.org/, doi:10.1016/j.wear.2009.10.013.
[14] Z. Jia, Y. Tao, L. Sun, Y. Zhao, C.T. Liu, A novel multinary intermetallic as an active electrocatalyst for hydrogen evolution, Adv. Mater. 32 (21) (2020) 2000385 http://dx.doi.org/, doi:10.1002/adma.202000385.
[15] C. Lu, L. Niu, N. Chen, K. Jin, T. Yang, P. Xiu, Y. Zhang, F. Gao, H. Bei, S. Shi, Enhancing radiation tolerance by controlling defect mobility and migration pathways in multicomponent single-phase alloys, Nat. Commun. 7 (2016) 13564 http://dx.doi.org/, doi:10.1038/ncomms13564.
[16] S.Q. Xia, X. Yang, T.F. Yang, S. Liu, Y. Zhang, Irradiation Resistance in Al x CoCrFeNi High Entropy Alloys, JOM (2015) http://dx.doi.org/, doi:10.1007/s11837-015-1568-4.
[17] D. Raabe, C. Tasan C., H. Springer, K. Pradeep G., Design of a twinning-induced plasticity high entropy alloy, Acta Mater. (2015) http://dx.doi.org/, doi:10.1016/j.actamat.2015.04.014.
[18] F.F. Csikor, C. Motz, D. Weygand, M. Zaiser, S. Zapperi, Dislocation avalanches, strain bursts, and the problem of plastic forming at the micrometer scale, Science 318 (5848) (2007) 251–254 http://dx.doi.org/, doi:10.1126/science.1143719.
[19] A. Gali, E.P. George, Tensile properties of high- and medium-entropy alloys, Intermetallics 39 (2013) 74–78 http://dx.doi.org/, doi:10.1016/j.intermet.2013.03.018.
[20] B. Gludovatz, A. Hohenwarter, D. Catoor, E.H. Chang, E.P. George, R.O. Ritchie, A fracture-resistant high-entropy alloy for cryogenic applications, Science 345 (6201) (2014) 1153–1158 http://dx.doi.org/, doi:10.1126/science.1254581.
[21] P. Schall, I. Cohen, D.A. Weitz, F. Spaepen, Visualizing dislocation nucleation by indenting colloidal crystals, Nature 440 (7082) (2006) 319–323 http://dx.doi.org/, doi:10.1038/nature04557.
[22] V. Yamakov, D. Wolf, M. Salazar, S.R. Phillpot, H. Gleiter, Length-scale effects in the nucleation of extended dislocations in nanocrystalline Al by molecular-dynamics simulation, Acta Mater. 49 (14) (2001) 2713–2722 http://dx.doi.org/, doi:10.1016/S1359-6454(01)00167-7.
[23] Y.T. Zhu, X.Z. Liao, X.L. Wu, Deformation twinning in nanocrystalline materials, Prog. Mater. Sci. 57 (1) (2012) 1–62 http://dx.doi.org/, doi:10.1016/j.pmatsci.2011.05.001.
[24] T.G. Langdon, Grain boundary sliding as a deformation mechanism during creep, Philos. Mag. 22 (178) (2006) 689–700 http://dx.doi.org/, doi:10.1080/14786437008220939.
[25] Y. Wei, A. Bower, H. Gao, Recoverable creep deformation and transient local stress concentration due to heterogeneous grain-boundary diffusion and sliding in polycrystalline solids, J. Mech. Phys. Solids 56 (4) (2008) 1460–1483 http://dx.doi.org/, doi:10.1016/j.jmps.2007.08.007.
[26] Z. Liu, G. Han, S. Sohn, N. Liu, J. Schroers, Nanomolding of Crystalline Metals: the smaller the easier, Phys. Rev. Lett. 122 (3) (2019) http://dx.doi.org/, doi:10.1103/PhysRevLett.122.036101.
[27] Z. Liu, One-step fabrication of crystalline metal nanostructures by direct nanoimprinting below melting temperatures, Nat. Commun. 8 (2017) 14910 http://dx.doi.org/, doi:10.1038/ncomms14910.
[28] J. Brechtl, S. Chen, C. Lee, Y. Shi, R. Feng, X. Xie, D. Hamblin, A.M. Coleman, B. Straka, H. Shortt, R.J. Spurling, P.K. Liaw, A review of the Serrated-flow phenomenon and its role in the deformation behavior of high-entropy alloys, Metals (Basel) 10 (8) (2020) 1101 http://dx.doi.org/, doi:10.3390/met10081101.
[29] S. Zhao, Z. Li, C. Zhu, W. Yang, M.A. Meyers, Amorphization in extreme deformation of the CrMnFeCoNi high-entropy alloy, Sci. Adv. 7 (5) (2021) 3108–3137 http://dx.doi.org/, doi:10.1126/sciadv.abb3108.
[30] Z. Lei, X. Liu, W. Yuan, W. Hui, Z. Lu, Enhanced strength and ductility in a high-entropy alloy via ordered oxygen complexes, Nature 563 (7732) (2018) http://dx.doi.org/, doi:10.1038/s41586-018-0685-y.
[31] H. Huang, Y. Wu, J. He, H. Wang, X. Liu, K. An, W. Wu, Z. Lu, Phase-transformation ductilization of brittle high-entropy alloys via metastability engineering, Adv. Mater. 29 (30) (2017) 1701678.1–1701678.7 http://dx.doi.org/, doi:10.1002/adma.201701678.
[32] L. Romano, J. Vila-Comamala, M. Kagias, K. Vogelsang, H. Schift, M. Stampanoni, K. Jefimovs, High aspect ratio metal microcasting by hot embossing for X-ray optics fabrication, Microelectron. Eng. 176 (2017) 6–10 http://dx.doi.org/, doi:10.1016/j.mee.2016.12.032.
[33] P. Braun, K. Durst, A multiple length-scales Nanoimprinting approach on Nanocrystalline and strongly deformed CuZn30 alloys, Sci. Rep. 10 (1) (2020) 2454 http://dx.doi.org/, doi:10.1038/s41598-020-58874-y.
[34] Q. Su, J. Xu, C. Wang, D. Shan, B. Guo, The Fabrication of Micro-Array Channels with the Ultrafine-Grained LZ91 Mg-Li Alloy by Micro-Embossing, Micromachines (Basel) 9 (2) (2018) http://dx.doi.org/, doi:10.3390/mi9020055.
[35] X. Liu, K. Li, J. Shen, F. Gong, Hot embossing of moth eye-like nanostructure array on transparent glass with enhanced antireflection for solar cells, Ceram. Int. (2021) http://dx.doi.org/, doi:10.1016/j.ceramint.2021.03.159.
[36] X. Shan, H. Maw, R. Tjeung, S. Ling, C. Lu, R. Jachowicz, Microstructure formation on low temperature co-fired ceramic green substrates using micro embossing, Microsyst. Technol. 14 (9) (2008) 1405–1409 http://dx.doi.org/, doi:10.1007/s00542-008-0561-z.
[37] G. Kumar, H.X. Tang, J. Schroers, Nanomoulding with amorphous metals, Nature 457 (7231) (2009) 868–872 http://dx.doi.org/, doi:10.1038/nature07718.
[38] Y.H. Liu, G. Wang, R.J. Wang, M.X. Pan, W.H. Wang, Super plastic bulk metallic glasses at room temperature, Science 315 (5817) (2007) 1385–1388 http://dx.doi.org/, doi:10.1126/science.1136726.
[39] J. Ma, C. Yang, X. Liu, B. Shang, Y. Yang, Fast surface dynamics enabled cold joining of metallic glasses, Sci. Adv. 5 (11) (2019) eaax7256 http://dx.doi.org/, doi:10.1126/sciadv.aax7256.
[40] L. Zhang, L. Qiu, Q. Zhu, X. Liang, J. Huang, M. Yang, Z. Zhang, J. Ma, J. Shen, Insight into efficient degradation of 3, 5-dichlorosalicylic acid by Fe-Si-B amorphous ribbon under neutral condition, Appl. Catal. B (2021) 120258 http://dx.doi.org/, doi:10.1016/j.apcatb.2021.120258.
[41] Y. Yan, C. Wang, Z. Huang, J. Fu, Z. Lin, X. Zhang, J. Ma, J. Shen, Highly efficient and robust catalysts for the hydrogen evolution reaction by surface nano engineering of metallic glass, J. Mater. Chem. A 9 (9) (2021) 5415–5424 http://dx.doi.org/, doi:10.1039/D0TA10235K.
[42] J. Fu, J. Yang, K. Wu, H. Lin, W. Wen, W. Ruan, S. Ren, Z. Zhang, X. Liang, J. Ma, Metallic glue for designing composite materials with tailorable properties, (2021). http://dx.doi.org/ 10.1039/D1MH00521A
[43] H. Li, Z. Li, J. Yang, H.B. Ke, B. Sun, C.C. Yuan, J. Ma, J. Shen, W.H. Wang, Interface design enabled manufacture of giant metallic glasses, Sci. China Mater. 64 (4) (2021) 964–972 http://dx.doi.org/, doi:10.1007/s40843-020-1561-x.
[44] X. Li, D. Wei, J. Zhang, X. Liu, Z. Li, T. Wang, Q. He, Y. Wang, J. Ma, W. Wang, Ultrasonic plasticity of metallic glass near room temperature, Appl. Mater. Today 21 (2020) 100866 http://dx.doi.org/, doi:10.1016/j.apmt.2020.100866.

[45] X. Liang, X. Zhu, X. Li, R. Mo, Y. Liu, K. Wu, J. Ma, High-entropy alloy and amorphous alloy composites fabricated by ultrasonic vibrations, Sci. China: Phys., Mech. Astron. 63 (2020) 1–5 http://dx.doi.org/, doi:10.1007/s11433-020-1560-4.

[46] Z. Wang, C. Wang, Y.-.L. Zhao, J.-.J. Kai, C.-.T. Liu, C.-.H. Hsueh, Fatigue studies of CoCrFeMnNi high entropy alloy films using nanoindentation dynamic mechanical analyses, Surf. Coat. Technol. 410 (2021) 126927 http://dx.doi.org/, doi:10.3390/met10081101.